Frontal cortex norepinephrine, serotonin, and dopamine dynamics in an innate fear-reward behavioral model

Jen-Hau Yang[1,9], Aakash Basu[2], Rong-Jian Liu[1], Stephanie M. Staszko[1], Abigail L. Yu[1], Jocelyne Rondeau[1], Samira Glaeser-Khan[1], Jiesi Feng[4-6], Yulong Li[4-6], Alicia Che[1,7-8], Alfred P. Kaye[1, 7-8]

1. Yale University Department of Psychiatry, New Haven, CT
2. Yale University Interdepartmental Neuroscience Program, New Haven, CT
3. State Key Laboratory of Membrane Biology, Peking University School of Life Sciences, Beijing 100871, China
4. PKU-IDG/McGovern Institute for brain research, Beijing 100871, China
5. Peking Tsinghua Center for Life Sciences, Academy for Advanced Interdisciplinary Studies, Peking University, Beijing 011871, China
6. Chinese Institute for Brain Research, Beijing, 102206, China
7. Wu Tsai Institute, New Haven, CT
8. VA National Center for PTSD Clinical Neuroscience Division, West Haven, CT
9. National Sun Yat-Sen University Doctoral Program of Clinical and Experimental Medicine, Kaohsiung, Taiwan.

Corresponding author: Alfred P. Kaye. Email: alfred.kaye@yale.edu

Abstract

Animals must survive by foraging for food in an uncertain and dangerous world. Experimental tasks such as Pavlovian learning have yielded insights into how neural circuits balance these conflicting motivational drives. Neuromodulators play a fundamental role in this process, enabling flexible switching between motivational drives. The question of how neuromodulators synergistically encode motivational state is thus fundamental to systems neuroscience, yet the interplay between these neuromodulators during naturalistic decision making are not fully understood. Here, we developed a naturalistic approach/avoidance task in mice involving a tradeoff between seeking reward versus safety in the presence of looming predation risk. We utilized multi-fiber photometry, computational behavior tracking, and slice electrophysiology to understand the . Mice that experienced looming stimuli showed increased c-fos expression in

regions including frontal cortex, locus coeruleus, and ventral tegmental area, but decreased expression in dorsal raphe nucleus. Moreover, by using multi-fiber photometry combined with GPCR-based sensors, we found that cortical norepinephrine (NE) plays a more prominent role in encoding looming threats while dopamine (DA) represents reward and threat. In contrast, serotonin (5HT) dynamic negatively correlates to both emotional valences. To begin to understand neuromodulatory interactions, we used *ex vivo* slice physiology to understand 5HT impact on spontaneous firing of locus coeruleus NE neurons. In conclusion, monoamines such as NE, DA, 5HT can converge in their encoding of naturalistic motivated behaviors as well as dissociate from one another. By utilizing this approach, interactions between innate fear and incentive for food may be delineated in terms of basis in neurochemical signaling events during natural behavior, and may contribute to the understanding of neural mechanisms underlying emotional disorders including anxiety and post-traumatic stress disorder.

Introduction

To survive, animals must forage for food under predatory risk. Efficient adaptation to this motivational conflict is therefore crucial (Dennis et al., 2021). Threat signals induce immediate defensive behavior including fight or flight, and these innate emotional responses are conserved across species and developmental stages (Silva et al., 2016; Evans et al., 2019). To study the neural mechanisms underlying this process, aversive stimuli such as foot shocks, predator odors, startle tone, and looming have been widely used in rodent research (Adolphs, 2013; Ganella & Kim 2014; Bedoya-Perez et al., 2019). Considering ethological relevance, looming stimulus has emerged as a more naturalistic fear stimulus because it utilizes vision, which is the most useful sensory modality for detecting aerial predators, and it reliably induces rapid innate fear responses including freezing and escaping (Yilmaz & Meister, 2013; Evans et al., 2018). Due to its complexity, looming-induced defensive behavior is suggested to be regulated by multiple brain areas including amygdala, thalamus, superior colliculus, frontal cortex (Zhao et al., 2014; Wei et al., 2015; Shang et al., 2015, 2018; Hu et al., 2017; Evans et al., 2018; Salay et al, 2018; Vander Weele et al., 2018; Fratzl et al., 2021), as well as neuromodulator synthesizing areas such as locus coeruleus (LC), ventral tegmental area (VTA) and dorsal raphe nucleus (DRN) (Huang et al., 2017; Li et al., 2018; Zhou et al., 2019; Barbano et al., 2020). While an increasing number of studies have focused on investigating the neural circuits for looming-induced defensive behavior, how animals cope with the motivational conflict between avoiding threats and approaching available rewards remains elusive.

Naturalistic decision making requires continuous evaluations between positive and negative valence, which in turn lead to the exertion of approach or avoidance behaviors. This conflict process has been conceptualized as approach/avoidance decision making, which has been widely used as a paradigm for assessing anxiety-related behaviors in humans and animals (Ito & Lee, 2016; Kirlic et al., 2017; La-Vu et al., 2020; Chen et al., 2022). In most studies, however, subjects are often required to learn the contingency of certain actions that lead to reinforcer or punishment (i.e., instrumental conditioning), or the association between cues and punishment without simultaneous reward across discrete trials (e.g., go/no-go tasks). More recently, researchers have sought to use more ethologically relevant stimuli that trigger innate responses in conflict tasks (Miller et al., 2019; Zambetti et al., 2019, 2022), but animals in these experiments are usually food/water deprived, leading to biased intrinsic value and risk assessment (Ito & Lee, 2016; Burnett et al., 2016). The question of how neuromodulators synergistically modulate naturalistic risk-reward conflicts remains largely unresolved.

Individual neuromodulators including norepinephrine (NE), dopamine (DA), and serotonin (5HT), are known to play fundamental yet distinct roles in processing and switching between motivational drives. For example, NE represents exploration-exploitation tradeoffs or uncertainty within threat (Yu & Dayan, 2005; Sciolino et al., 2022; Basu et al., BioRxiv), DA canonically represents reward prediction errors and motivated behavior (Schultz, 2010, 2016; Salamone & Correa, 2012; Zald & Treadway, 2017; Salamone et al., 2018), and 5HT functionally modulates emotional motives (Marcinkiewcz et al., 2016; Huang et al., 2017; Ren et al., 2018). Among subcortical and cortical transmission networks, the prefrontal cortex stands out as a critical region that receives convergent neuromodulatory inputs to process complex cognitive functions

(Cools & Arnsten, 2022). For instance, the medial prefrontal cortex (mPFC) has been shown to encode sensory salience by incorporating neuromodulatory inputs (Ventura et al., 2008; Kim et al., 2018; Ritter et al., BioRxiv). Consequently, the mPFC is an ideal target area for assessing multiple neuromodulatory effects in mice performing an approach/avoidance conflict task.

In this study, we first identified looming-related regions of interest by whole-brain cFos screening, and recorded multiple neuromodulators simultaneously in freely moving mice in a naturalistic conflict decision making task by using multi-fiber photometry with GPCR activation-based (GRAB) sensors. The GRAB sensors are genetically encoded neuromodulator indicators, enabling direct measurement of evoked neuromodulator release *in vivo* (Sun et al., 2018, 2020; Feng et al., 2019; Wan et al., 2021). We found that DA, NE, and 5HT each showed distinct encoding of innate reward and threat during aspects of the task, while remaining highly correlated at other times. This work contributes to the understanding of the pathology of anxiety and post-traumatic stress disorder (Kaye & Krystal, 2020).

Results

Approach/avoidance behavior in an innate emotional conflict task

To investigate the motivational conflict between foraging for reward and environmental threats, we developed a naturalistic approach/avoidance task in mice (**Figure 1A**). In this task, freely moving mice were allowed to explore in a rectangle arena for reward readily upon licking the spout (i.e., approach, **Figure 1B**) or to flee and hide in a red-tinted shelter from visual looming stimuli (i.e., avoidance, **Figure 1C**). The looming stimulus was displayed as a video of a quickly expanding black disk above the arena to simulate approaching aerial predator, which reliably caused innate fear responses (Yilmaz & Meister, 2013; Evans et al., 2018). Looming was randomly presented twice in each of 5 daily sessions. All behaviors were recorded throughout each 20-25 min session and analyzed offline with Matlab and Deeplabcut (**Figure S2A&B**, Mathis et al, 2018). At the first looming stimulus, 96% of mice immediately exhibited classic fear responses (freezing or escaping), but this percentage decreased to 52% at the 10th looming stimulus (**Figure 1D**). In contrast, the number of licks within the first 180 seconds increased significantly across days ($F(4, 120) = 4.084$, $p < 0.005$), and multiple comparisons with adjusted p value further indicated significant differences at Day 1 versus Day 3 and Day 1 versus Day 4 (both $p < 0.05$, **Figure 1E**). There was no sex difference in total licks between male (178.7 ± 38.6) and female (225.1 ± 51.1, $p = 0.17$, data not shown). In this conflict task, mice showed adaptive behavior in a manner of decreased looming-induced fear responses and increased number of licks, indicating a natural flexible switch of behavior from more escaping to more reward seeking (**Figure 1F**). To determine how looming threats directly impact licking behavior, we analyzed the events where the looming was displayed while the mouse was licking or not (**Figure 1G**). The area under the curve (AUC) of each daily psychometric function in likelihood toward the next lick increased across days, suggesting an elevated tendency to overcome the looming threat over time. These findings collectively demonstrated an adaptive behavior in mice performing the conflict task, akin to the vigorous flexibility seen in animals foraging under predatory threats in the wild.

Prefrontal NE encodes looming threats, and DA encodes reward bouts

We conducted an unbiased whole-brain cFos mapping (Park et al., 2018) to identify looming-related regions of interest (**Figure S1**). The cFos expression in mice who experienced one-time looming stimulus (looming group) revealed increased neural activity in LC - a major NE synthesizing area, VTA - a major DA synthesizing area, as well as mPFC, specifically prelimbic area. In contrast, the DRN - a major 5HT synthesizing area showed decreased cFos expression (**Figure S1B&C**). Considering the finding of increased cFos expression in LC and VTA, we next sought to directly measure *in vivo* NE and DA release at mPFC in mice performing the conflict task. The mPFC is a major hub that receives numerous neuromodulatory inputs and processes higher cognitive functions including decision making (Cools & Arnsten, 2022), so we reasoned that mPFC would show diverse neuromodulatory signals in our task. In this study, cortical NE and DA dynamics were measured by using G-protein-coupled receptor activation based (GRAB) sensors ($GRAB_{NE}$: AAV9-hSyn-NE2h; $GRAB_{DA}$: AAV9-hSyn-DA3m), which are fluorescent indicators of neuromodulator release (Sun et al., 2018, 2020; Feng et al., 2019). Accordingly,

multi-fiber photometry is achieved by unilateral injections of $GRAB_{NE}$ or $GRAB_{DA}$ into each side of mPFC, thereby enabling both NE and DA recording simultaneously in the same animal (**Figure 2A&B**). The effectiveness of GRAB sensors *in vivo* has been verified pharmacologically by NE reuptake inhibitor and DA reuptake inhibitor treatments in our lab (unpublished data). Time-locked looming- and reward-related NE/DA traces were compiled by aligning the event onset time (t = 0, **Figure 2**), and a one-way ANOVA analysis for event-related NE df/f revealed a significant main effect in looming events across days (**Figure 2D**, $F(4, 100) = 2.939$, $p < 0.05$, multiple comparisons indicated significant difference between Day 1 vs. Day 4, $p < 0.05$) and reward-bout events (**Figure 2G**, $F(4, 92) = 5.211$, $p < 0.001$, and significant Day 2 vs. Day 4, $p < 0.05$; and Day 2 vs. Day 5, $p < 0.001$). On the other hand, DA dynamics showed no day main effect in looming (**Figure 2J**, $F(4, 46) = 0.2839$, $p = 0.89$), but a significant main effect in reward bout (**Figure 2M**, $F(4, 42) = 3.748$, $p < 0.05$, and significant Day 1 vs. Day 5, $p < 0.05$). Overall, the averaged mPFC NE dynamic plays a more prominent role in encoding looming threats over reward bouts (**Figure 2E&H**), whereas mPFC DA encodes reward bouts, especially in early days (**Figure 2K&N**).

Prefrontal NE is activated during threat exposure

Looming-evoked freezing and escaping have been previously shown to be promoted by divergent pathways (Salay et al., 2018; Shang et al., 2018), it is thus inferred that the same threat signal may trigger dissociative neuromodulatory dynamics corresponding to different behavioral response types. In this task, looming-evoked fear responses were categorized as freezing, escaping, and no response (**Figure 3A&B**). Overall, mice predominantly showed more freezing (57%) than escaping (21%) and no response (22%), and increased no response was associated with shorter latency to next lick (**Figure 3C**). Also, we found that male mice tend to freeze more to the looming stimuli compared with female mice (**Figure 3D**). By synchronizing photometry and behavioral tracking data, we next assess neuromodulatory effects on the different response types (**Figure 3E&F, S2**). Within a 15s window after looming onset, a one-way ANOVA revealed a significant response-type main effect in mPFC NE activity ($F(2, 207) = 4.901$, $p < 0.01$) and in DA ($F(2, 99) = 3.231$, $p < 0.05$). In NE activity, multiple comparisons further indicated significant differences between freezing and escaping ($p < 0.01$). In contrast, multiple comparisons in DA activity revealed no significant differences in freezing versus escaping ($p = 0.17$) or freezing versus no response ($p = 0.08$). This finding implicated that mPFC NE dynamic represents threat signals due to a fact that freezing mice kept exposed to looming compared to ones that ran away and hid in a shelter (**Figure 3E&F**).

Prefrontal 5HT activity is negatively correlated to looming threats and reward

Next, we sought to investigate the role of mPFC 5HT in the conflict task. We hypothesized that looming threats may reduce mPFC 5HT activity, based on decreased cFos expression in DRN, a main synthesis source of 5HT, in the looming group (**Figure S1**). In addition, a previous study indicated that activation of DRN 5HT neuron blocked looming-evoked fear responses (Huang et al., 2017). In order to enhance the motivational conflict, we added a pure-tone cue which indicates reward availability and potential looming stimuli, creating more confined conflict epoches to the same approach/avoidance task paradigm (**Figure 4A**). This ensured that reward

availability was restricted to be simultaneous with threat presentation instead of free availability as in previous experiments. In this 8-day task, mice were trained to associate the tone-on to reward in the first 4 days (training day T1 to T4), and the looming were added through day 5 to 8 (looming day L1 to L4, **Figure 4B&C**). Behaviorally, compared to well-trained day T1, mice licked significantly fewer on L1 ($p < 0.05$, planned comparisons) while keeping their high hit rate unchanged across all four looming days (all $p > 0.05$), suggesting that mice were able to maintain the accuracy in obtaining reward under looming threats (**Figure 4D**). Next, to investigate the role of 5HT in this task, mice injected with a $GRAB_{5HT}$ sensor (AAV9-hSy-5HT3.5(h-S06)) in mPFC were assessed. Although one-way ANOVA revealed no significant day-by-day main effects on 5HT dynamic changes on looming (**Figure 4F**, $F(3, 38) = 1.260$, $p = 0.30$) nor bout events (**Figure 4I**, $F(7, 75) = 1.331$, $p = 0.25$), 5HT showed consistent time-locked decrease to both looming and reward on individual trials that do not change over time (**Figure 4G&J**). Regarding looming-induced behavioral responses, a one-way ANOVA revealed significant fear-response main effect on 5HT release ($F(2,81) = 5.843$, $p < 0.005$), specifically between freezing and escaping ($p < 0.01$, **Figure 4K**). Lastly, we sought to investigate how looming stimuli and licking behavior affect the bout signal in 5HT (**Figure 4L**). Before looming stimuli were introduced, the pure reward signal encoded by mPFC 5HT showed an immediate decrease after reward bout onset and rebounded to baseline. Interestingly, after looming stimuli were added, the bout-related signals showed divergent patterns according to whether the mouse kept licking or not (**Figure 4L**). Together, these results suggested that mPFC 5HT is negatively correlated to both negative and positive valences in a behavior- and time-dependent manner.

NE, DA, and 5HT showed distinct encodings of negative and positive valences

To better understand the neuromodulatory effects of NE, DA, and 5HT in totality, we compared their time-locked dynamics on looming and reward bout events across groups (**Figure 5**). In looming-evoked df/f, a one-way ANOVA revealed significant neuromodulator main effect ($F(2, 44) = 58.93$, $p < 0.0001$) on immediate activity (t = 0.5 to 1.5s) with stronger NE activity compare to DA and 5HT (multiple comparisons, both $p < 0.001$). In the later activity (t = 17 to 20s), we found a significant neuromodulator main effect ($F(2, 44) = 142.7$, $p < 0.0001$) and significance of all three multiple comparisons (all $p < 0.001$). Similarly, in bout-related df/f, there was a significant neuromodulator main effect on both immediate ($F(2, 44) = 44.08$, $p < 0.0001$) and later activity ($F(2, 44) = 9.842$, $p < 0.0001$). Multiple comparisons further revealed a significantly stronger immediate response in DA versus NE ($p < 0.01$) and DA versus 5HT ($p < 0.001$), and NE versus 5HT ($p < 0.001$) in immediate activity, and both NE and DA were significantly stronger than 5HT (both $p < 0.005$) in later activity. Next, we aimed to determine whether the reward history would have an impact on dynamic changes by assessing the traces between the first 10 versus last 10 reward bouts. Both mPFC DA and NE showed an immediate peak at the first 10 bouts, and each trace was divergent from one in the last 10 bouts (**Figure S3A&B**). Collectively, these results suggested that NE plays a more prominent role representing negative valence, whereas DA encodes reward bout, and 5HT is negatively associated with both valences (**Figure 5A&6**).

5HT modulates LC NE neuron spikes

Another important question is how neuromodulators interact with each other to modulate complex emotional behaviors. To determine the direct interactions between NE and 5HT, we conducted an *ex vivo* slice electrophysiology recording of LC NE neurons with 5HT-related treatments (**Figure 7A & S4**). Spontaneous spikes in LC NE neurons were significantly increased after bath-applied 5HT ($p < 0.05$) and a $5HT_2$ receptor agonist DOI ($p < 0.05$, **Figure 7B&C**). Notably, we found sub-populations of LC NE neurons showed no change or decreased firing rate to 5HT and DOI treatments (**Figure 7D&E**). In sum, these findings suggest a heterogeneity in LC NE neurons interacting with 5HT systems.

Discussion

In this study, we used multi-fiber photometry to simultaneously record multiple neuromodulators at mPFC in mice performing a conflict task. The primary findings are, firstly, the development of a naturalistic decision making task to assess the motivational conflict between reward-seeking and threat-avoiding behaviors. Secondly, we found that NE plays a more prominent role in encoding negative valence (i.e., visual looming threats), whereas DA encodes positive valence (i.e., reward bouts). In contrast, 5HT appears to be negatively correlated with both valences. Also, the results from slice physiology demonstrated that 5HT regulates LC NE neurons in a population-dependent manner, providing supportive evidence of the crosstalk between NE and 5HT systems.

A key challenge in behavioral neuroscience is to design experimental paradigms that are applicable to real-world scenarios (Dennis et al., 2021; Zambetti et al., 2022; Miller et al., 2019). Recently, looming has emerged as a more ecological stimulus because it is innocuous and reliably triggers rapid innate defensive behaviors (Yilmaz & Meister, 2013; Evans et al., 2018). In this study, a reward component was additionally implemented on the premise of mimicking the natural foraging behavior under predator risk. Over sessions, we found that mice substantially suppressed the fear responses to the looming threat and increased the tendency to seek for reward, while maintaining high accuracy to reward availability. This adaptive behavior is crucial for survival because animals need to conserve energy from unnecessary escaping responses and exert effective exploitation of scarce resources (Evans et al., 2019; Dennis et al., 2021).

Looming-evoked fear responses have been shown to involve complex sensory transmissions and neuromodulatory pathways (Huang et al., 2017; Shang et al., 2018; Salay et al., 2018; Feng et al., 2019; Zhou et al., 2019). By using multi-fiber photometry combined with GRAB sensors, we directly measured the release of multiple neuromodulators *in vivo* simultaneously, and the results indicate looming increased mPFC NE and DA but decreased 5HT activities. These changes in dynamics are congruent to our whole-brain cFos experiment (**Figure S1**) and previous studies. The mPFC receives dense LC NE projections (Florin-Lechner et al., 1996; Marzo et al., 2014; Chandler et al., 2014), and this pathway has been shown to regulate fear-related learning and memory (Giustino & Maren, 2018). Agreeing with a previous finding of looming-triggered NE activity (Feng et al., 2019), our results further indicate that mPFC NE represents a threat signal by maintaining elevated levels during exposure to looming (i.e. mouse freezing). Also, mPFC NE showed a biphasic dynamic to reward bout onset, which is consistent with the pattern of firing rate in LC NE neurons responding to reward action in a monkey single-unit recording study (Varazzani et al., 2015). Notably, mPFC NE may represent reward prediction signal suggested by significant day-by-day change in bout (**Figure 2G**), providing supportive evidence of the emerging role of NE in encoding prediction error (Schultz & Dickinson 2000; Sciolino et al., 2022; Basu et al., BioRxiv; Su & Cohen, BioRxiv). Compared to NE, mPFC DA is more prominent in encoding reward signals, especially in early days (**Figure 2M** & **Figure 5**). The event-related increase in both looming and reward bout is in accord with the role of DA in encoding stimulus salience (Ungless, 2004; Schultz, 2010). In sum, our

findings demonstrate a dissociable role between mPFC NE and DA in representing looming threats and reward respectively, with a similar dynamic pattern overall (Ranjbar-Slamloo & Fazlali, 2020).

In contrast, 5HT showed decreased activity to both looming and reward bout. This finding is surprising because previous studies have suggested that DRN 5HT neurons are activated at reward intake and to reward-predicting cues (Liu et al, 2014; Cohen et al., 2015; Li et al., 2016; Matias et al., 2017; Ren et al., 2018). On the other hand, unlike reward signals, the results of DRN 5HT dynamic change to punishment are mixed. Studies reported DRN 5HT neurons have no response to aversive stimuli including timeout period, quinine, and foot shock (Liu et al., 2014; Li et al., 2016), but population-dependent excited or inhibited firing rate to air puff (Cohen et al., 2015). More recently, one study suggests that this punishment-evoked dissociation DRN 5HT is circuit-dependent, in which the central amygdala-projecting neurons were activated, whereas the orbitofrontal cortex-projecting neurons were inhibited, toward foot shock (Ren et al., 2018). Together, these discrepancies could be due to the complicated interactions of other neuromodulators (e.g., GABA and glutamate) and heterogeneous 5HT sub-receptor pathways are involved (Szabo & Blier, 2001; Masse et al., 2006; Ortega et al., 2012; Fernandez-Pastor et al., 2013; Liu et al., 2014; Delcourte et al., 2021), therefore future studies with more synaptic-specific approaches are required to fully explain the 5HT mechanisms underpinning behavior and cognition.

The finding of increased spontaneous spikes in LC NE neurons after 5HT-related treatments from our *ex vivo* slice physiology work confirms the direct 5HT regulations on LC NE neurons. While studies have shown that LC NE neurons receive inhibitory inputs from DRN 5HT innervating neurons (Pickel et al., 1977; Leger & Descarries, 1978; Aston-Jones et al., 1991; Kaehler et al., 1999), several *in vivo* studies reported mixed results that this mechanism being regulated by $5HT_1$ (Clement et al., 1992), $5HT_{2A}$ (Clement et al., 1992; Szabo & Blier, 2001), or $5HT_3$ receptors (Ortega et al., 2012). However, the effects of these 5HT administrations on LC NE neurons may be confounded by the inputs of DRN 5HT projecting neurons. To eliminate direct inputs from DRN, we thus recorded the spontaneous activity from LC slices and bath-application with 5HT treatments. We found that 5HT, as well as a $5HT_2$ agonist DOI, applications reliably activated spontaneous spikes in LC NE neurons. And the 5HT-induced change in firing rate depends on the sub-population in LC NE neurons, implicating that 5HT regulation may indirectly influence a subset of LC NE neurons via GABAergic interneurons (Aghajanian et al., 1990; Aghajanian & Marek, 1999). Nonetheless, further studies are required to have a comprehensive understanding of how 5HT regulates LC NE neurons.

In summary, this study advanced the understanding of the involvements of multiple neuromodulators in an adaptive behavior in a motivational conflict task. In addition to NE, DA, and 5HT being investigated in this study, other neuromodulators such as acetylcholine (Zhu et al., 2018), GABA (Zhou et al., 2019), and glutamate (Barbano et al., 2020) are shown to be involved in this approach/avoidance behaviors. One future direction of our study is to examine the roles of other neuromodulators and neuropeptides in a naturalistic behavior. The looming-induced innate fear responses, which are conserved across species and different developmental ages (Schiff et al., 1962; Nanez, 1988; van der Weel & van der Meer, 2009), in

this task may provide insights of the neural mechanisms underlying emotional disorders such as anxiety and post-traumatic stress disorder (Kaye & Krystal, 2020).

Materials and Methods

Animals

A total of 63 (male = 36, female = 27) adult C57BL/6J mice (Jackson Laboratory, 8 – 10 weeks old at arrival) were used in this study. Animals were housed in groups of up to four mice per cage on a 12/12-h light–dark cycle with lights off at 19:00. Water and food were provided *ad libitum* in home cages. All procedures were performed in accordance with the regulations of NIH guidelines and the Institutional Animal Care and Use Committee at Yale University.

Apparatus

The behavior experiment was performed in a rectangular box (60 x 20 x 30 cm) built by clear acrylic sheets (adapted from Evans et al., 2018). A red-tinted acrylic shelter (10 x 19 x 13 cm) was placed at one end of the arena, and the reward spout (20 gauge blunt dispensing tips, CMLsupply) was inserted through a small drilled hole (4 cm from floor) on the wall at the other end. Each reward delivery was 3 μL of 50% Ensure (milk chocolate flavor, Abbott) mixed with water, and was dispensed via reward spout upon licks. Licks to the spout were detected by a custom made lickometer consisting of a dispensing tip electrically connected to a capacitive touch sensor and an Arduino redboard (Sparkfun Electronics). Reward delivery was controlled by scripts written in Presentation software (Neurobehavioral Systems, Inc.) via a DAQ card (USB-201, Measurement Computing) and a solenoid valve (McIntosh Controls Corp). A 27-inch monitor (1,920 x 1,080, Samsung SR35) was held facing down to the arena (60 cm from arena floor) to present visual looming stimuli. The looming stimulus was a video of a dark quick-expanding disk (full disk diameter 1,000 pixels) on white background generated by custom scripts written in Matlab (2021a, MathWorks, Inc.). A white noise generator (Homedics) set at 55-60 dB was used during behavioral experiments. Mouse behavior in each daily session was recorded by a camera (LifeCam HD-3000, Microsoft) mounted on the display monitor above the arena. The entire task structure—including lick detection and reward delivery—was automated and logged using custom scripts written in Presentation software.

Approach/avoidance task

Mice were handled and pre-fed with 1 mL 50% Ensure solution in home cages for at least two days prior to behavioral experiments. Food and water were available in home cages throughout the study. The approach/avoidance task consisted of a one-day habituation and 5 approach/avoidance days. In each daily session, mice were firstly placed in a bedded empty cage with fiber cord connected to the optic fiber implant for 5 minutes to habituate the cables. Mice were then placed into the arena for 15 minutes without reward or looming stimulus on habituation day. On the following approach/avoidance days (25-30 min), reward was available upon licking the spout with a 250 ms inter-reward-interval due to the nature of rapid mouse licks (8-12 Hz), and looming stimuli were randomly displayed twice a day from the monitor above. One looming stimulus consisted of 6-10 cycles of a quickly expanding dark disk, and each cycle contained 600 ms expanding period, 400 ms staying at maximal (11.5° visual angle from mouse), and 800 ms inter-cycle-interval. Looming stimuli were displayed only when the mouse

was not in the shelter. The photometry system was calibrated and started when the cord-connected mouse was placed in the empty cage and throughout each daily session. Separate bedded empty cages were used between male and female mice. The arena and shelter were cleaned with 70% ethanol between mice.

The tone version of the approach/avoidance task consisted of one habituation day (same as described above) and 8 experimental days. On day 1 to 4 (training days, T1 to T4, 20 min), mice were placed in the arena with rewards available only when a 5k Hz tone was on (75-80 dB). Licks during tone-on periods were rewarded and recorded as 'hits.' Tone-on durations (10, 15, …, 60s) and inter-tone-intervals (15, 16, …, 25s) were randomized with an averaged on/off ratio at around 63%. On day 5 to 8 (looming days, L1 to L4, 20 min), looming stimuli randomly presented twice a day only during tone-on periods. In tone-off periods, there was no reward or looming stimulus, and licks during which were recorded as 'misses.'

c-Fos whole brain mapping

Twelve C57BL/6 mice (6 males/6 females) of a new cohort were randomly assigned into a looming or home cage control group (each group n = 6, 3 males/3 females). Mice in the looming group were placed in the approach/avoidance arena for 10 minutes with one looming stimulus (6-10 cycles) presented at 5th minute (**Figure S1**). Mice, including those in the control group, were then removed to an empty cage individually without food or water and rested for two hours. After which, mice were deeply anesthetized with isoflurane and perfused transcardially with PBS with 10U/mL heparin (Sigma-Aldrich), followed by ice-cold 4% paraformaldehyde (Sigma-Aldrich). Brains were collected and fixed in 4% paraformaldehyde at 4℃ for 24 hours with gentle shaking. The samples were then washed in PBS and stored in 0.02% sodium azide (Sigma-Aldrich) in PBS, and were shipped to LifeCanvas for whole brain c-Fos imaging. Positive cFos cells were identified by expressing both cFos (642 nm) and neuronal nuclei protein (561 nm). The dataset contains c-Fos expressing cell densities from 1,678 distinct brain areas with an imaging resolution of 1.8 x 1.8 x 4 microns per voxel. Left and right hemispheres of the same region were combined and averaged. Data were analyzed offline by customized scripts in Matlab.

Surgery

Before optogenetic and photometry recording experiments, mice underwent a surgery of viral injection and fiber implementation as described previously (Basu et al). In brief, mice were anesthetized with 1-4% isoflurane (Covetrus, ME) in oxygen and secured in a stereotaxic frame. The scalp was first disinfected with sterile alcohol pads (Fisherbrand) and was partially removed to expose the dorsal aspect of the skull. The periosteum was gently removed, and the surface of the skull was cleaned with 0.9% saline. Bilateral injection sites were made by drilling through the skull at [AP] = +1.6 mm, [ML] = ±0.8 mm relative to bregma to expose the dura. Note the [ML] was adjusted from ±0.3 mm (above mPFC) to ±0.8 mm due to a 20º angle injection was applied to avoid the central sinus and to ensure space between two optic fibers (**Figure 2A&B**). For the NE-DA cohort in photometry experiments, 0.5 μL of $GRAB_{NE}$ (AAV9-hSyn-NE2h, WZ Biosciences) and $GRAB_{DA}$ (AAV9-hSyn-DA3m (DA3.3), WZ Biosciences) sensors were injected

into each side of mPFC respectively. The GRAB sensors injected into the left and right side of mPFC were counterbalanced between mice. Each virus was infused via a 5 μL Hamilton syringe (85N syringe, Hamilton, NV) targeted at depth [DV] = -1.4 mm with 20º angles. The injection rate was 0.1 μL per minute, and the syringe was left in place for an extra 5 minutes to minimize backflow of the injected solution. For the 5HT cohort, the $GRAB_{5HT}$ sensor (AAV9-hSyn-5HT2h, WZ Biosciences) was injected following the same procedures. After viral injection, 3 mm optic fibers (Neurophotometrics, Ltd.) were implanted at depth [DV] = -1.4 mm from brain surface with 20º angles bilaterally and were secured by dental cement (C&B Metabond; Parkell Inc.) which also covered the entire exposed skull. After removal from surgical apparatus, mice were treated with lidocaine (5 mg/kg, Covetrus, ME) and carprofen (5 mg/kg, Butler Animal Health) subcutaneously. Post-operatively, carprofen and lidocaine treatments were applied daily for two days, and followed by a four-week grace period for viral expression before behavioral experiment commencement.

Histology

After all experiments, mice were first deeply anesthetized with isoflurane and were perfused transcardially with ice-cold PBS followed by 4% paraformaldehyde (Sigma-Aldrich). Brains were carefully removed and post-fixed in 4% paraformaldehyde at 4℃ for at least 24 hours, and then switched to 30% sucrose solution until brain slicing. Frontal areas of the brains were sectioned coronally into 100 μm slices with a cryostat (Leica CM3050S) and mounted onto charged slides. Slides were covered by cover glass (Gold Seal, Thermo Scientific) with a mountant with DAPI (ProLong, Thermo Scientific), and then were imaged using a confocal microscope (Olympus FV3000) for fluorescence expression. The brightness and contrast of the images were adjusted appropriately in ImageJ to enhance the clarity of the area. Based on the histology, mice were excluded from analysis if fluorescence was not visible in mPFC region or a dislocation of fiber track from fluorescent areas.

Multi-fiber photometry recording

The same fiber photometry system was also used to measure the GRAB sensor fluorescence. Multi-fiber recording was achieved by connecting parallel patch cords to bilateral optic fiber implants in mice, enabling multi-channel readout of each sensor signal independently and simultaneously from both mPFC hemispheres. In each recording channel, light at the 470 nm excitation wavelength and a 415 nm isosbestic control was emitted from LEDs with 10% power and 20 Hz pulse frequency, and propagated to the optic fiber implants. Fluorescence emission from GRAB sensors was captured by an sCMOS camera at a frame rate of 40 Hz. The time-dependent fluorescence data were saved and analyzed offline by customized Matlab scripts.

Data Analyses

Behavioral data. All behavioral raw data including timestamps for licks, reward deliveries, and looming events were logged into text files by Presentation in each daily session. Data were pre-processed and analyzed by customized scripts written in Matlab. One reward

bout was defined as a train of licks within 5 seconds from the last lick. Looming events were aligned by the start of looming stimulus and reward bout events were aligned at the first lick of each bout (onset time, t = 0). Looming-induced escaping behavior was defined as mouse running and reached to shelter within the first 3 cycles of looming stimulus, whereas freezing behavior was defined as rigidness without any visible movements. In contrast, 'no response' to looming was defined as behaviors other than freezing and escaping, including but not limited to grooming, exploring, or licking. Additionally, mouse behavior was recorded throughout each daily session and analyzed by a supervised tracking system (Deeplabcut, Mathis et al., 2018) for precise position tracking per frame. The model was trained by feeding ~1,000 randomly selected frames, in which mice were manually labeled with the nose, left ear, right ear, central body, left side of body, right side of body, tail base, and tail end on the mouse (**Figure S2A**). The outputs generated by the well-trained network were analyzed by customized Matlab scripts.

Photometry data. GRAB sensor fluorescent signals were recorded and saved by Bonsai interface, and analyzed by customized scripts written in Matlab. In addition to histology examinations, certain sessions were excluded (NE: 20/125, DA: 6/60, 5HT: 4/88) due to motion artifacts caused by twisted patch cords during recording. For data processing, the 470 nm traces were firstly smoothed with a non-linear regression algorithm to correct the mild photobleaching effect in each day. To assess the event-related dynamics, the fluorescent signals were extracted with certain time windows aligned with event onset time (t = 0). The event-related fluorescence $\Delta F/F(t)$ was then calculated for each time bin *t* as:

$$\Delta F/F(t) = \frac{F(t) - F_0(t)}{F_0(t)}$$

where $F(t)$ is the fluorescence in time bin (50 ms each), and $F_0(t)$ is the baseline average signal ranging from -3 to -1.5 seconds from each event onset. To examine the day-by-day effects, all event-related signals in each session were averaged and plotted with 95% confidence intervals.

Ex vivo slice physiology

Brain slice preparation and electrophysiology recording procedures were similar to that described previously (Liu & Aghajanian, 2008). In brief, four C57BL/6 mice were used and their brains were placed in -4°C artificial cerebrospinal fluid (ACSF) in which sucrose (252 mM) replaced NaCl (sucrose-ACSF) to prevent cell swelling. Next, the brain tissue containing LC was sliced with 400 μm thickness using a vibratome (Leica VT1000S). Testing drugs were dissolved in ACSF and applied with a flow rate at 4 mL/min. A recovery period of ~1–2 hr was allowed before commencement of recording. To visualize the NE neurons in LC, an Olympus BX50WI microscope (x40 or x60 IR lens) with infrared differential interference contrast (IR/DIC) videomicroscopy (Olympus) was used. Whole-cell recordings were performed with an Axoclamp-2B amplifier (Axon Instruments). The output signal was low-pass-filtered at 3 KHz,

amplified x100 through Cyberamp, digitized at 15 kHz, and acquired by using pClamp 10.1/Digidata 1320 software (Axon Instruments). Postsynaptic currents were studied in the continuous single-electrode voltage-clamp mode (3-kHz low-pass filter cutoff frequency). After completion of recording, slices were transferred to 4% paraformaldehyde in 0.1 M phosphate buffer and stored overnight at 4°C. Slices were then processed with streptavidin conjugated to Alexa 594 (1/1,000; Invitrogen) for visualization of Neurobiotin-labeled cells.

Statistics

All statistics were performed in Matlab or GraphPad Prism (9.4.1). No statistical analysis was employed to determine sample sizes; however, they were similar to those used elsewhere in the field. For behavioral data statistical analyses, one-way analysis of variance (ANOVA) with repeated measures was used to analyze the behavioral parameters. Post-hoc analyses with adjusted alpha value were performed to assess the differences in certain time windows if the main effect was significant. To determine the differences between neuromodulatory traces related to events, the mean df/f was calculated with 95% confidence intervals generated using shuffled trial types for 1,000 times. Chi-square test and student's paired t-test were used to determine differences between treatments in slice physiology experiments. All data were presented as mean ± SEM or mean ± 95% confidence interval, and significance level was set at $\alpha = 0.05$ unless otherwise noted. Data plots were generated by Matlab or Prism, and diagrams were made with Adobe Illustrator (27.1.1) and Biorender (BioRender.com).

Data availability

The behavioral and photometry data, as well as customized codes written in Matlab and Presentation used in this study are available from the corresponding authors upon request.

References

Adolphs R. (2013). The biology of fear. *Curr Biol*, 23(2):R79-93

Aghajanian GK, Marek GJ. (1999). Serotonin and hallucinogens. *Neuropsychopharmacology*, 21(2 Suppl):16S-23S

Aghajanian GK, Sprouse JS, Sheldon P, Rasmussen K. (1990). Electrophysiology of the central serotonin system: receptor subtypes and transducer mechanisms. *Ann N Y Acad Sci*, 600:93-103

Aston-Jones G, Akaoka H, Charléty P, Chouvet G. (1991). Serotonin selectively attenuates glutamate-evoked activation of noradrenergic locus coeruleus neurons. *J Neurosci*, 11(3):760-9

Barbano MF, Wang HL, Zhang S, Miranda-Barrientos J, Estrin DJ, Figueroa-González A, Liu B, Barker DJ, Morales M. (2020). VTA Glutamatergic neurons mediate innate defensive behaviors. *Neuron*, 107(2):368-382

Basu A, Yang JH, Yu A, Glaeser-Khan S, Feng J, Krystal JH, Li Y, Kaye AP. (2022). Prefrontal norepinephrine represents a threat prediction error under uncertainty. *BioRxiv,* 2022.10.13.511463

Bedoya-Pérez MA, Smith KL, Kevin RC, Luo JL, Crowther MS, McGregor IS (2019). Parameters That Affect Fear Responses in Rodents and How to Use Them for Management. *Frontiers in Ecology and Evolution*, 7:136

Burnett CJ, Li C, Webber E, Tsaousidou E, Xue SY, Brüning JC, Krashes MJ. (2016). Hunger-Driven Motivational State Competition. *Neuron*, 92(1):187-201

Chandler DJ, Gao WJ, Waterhouse BD. (2014). Heterogeneous organization of the locus coeruleus projections to prefrontal and motor cortices. *Proc Natl Acad Sci USA*, 111(18):6816-21

Chen JA, Li S, Wang BX, Wu N, Li F, Li J. (2022). The effect of visually evoked innate fear on reward-associated conditional response and reversal learning in mice. *Physiol Behav*, 244:113648

Clement HW, Gemsa D, Wesemann W. (1992). Serotonin-norepinephrine interactions: a voltammetric study on the effect of serotonin receptor stimulation followed in the N. raphe dorsalis and the Locus coeruleus of the rat. *J Neural Transm Gen Sect*, 88(1):11-23

Cohen JY, Amoroso MW, Uchida N. (2015). Serotonergic neurons signal reward and punishment on multiple timescales. *Elife*, 4:e06346

Cools R, Arnsten AFT. (2022). Neuromodulation of prefrontal cortex cognitive function in primates: the powerful roles of monoamines and acetylcholine. *Neuropsychopharmacology*, 47(1):309-328

Delcourte S, Etievant A, Haddjeri N. (2021). Role of central serotonin and noradrenaline interactions in the antidepressants' action: Electrophysiological and neurochemical evidence. *Prog Brain Res*, 259:7-81

Dennis EJ, El Hady A, Michaiel A, Clemens A, Tervo DRG, Voigts J, Datta SR. (2020). Systems neuroscience of natural behaviors in rodents. *J Neurosci*, 41(5):911-919

Evans DA, Stempel AV, Vale R, Branco T. (2019). Cognitive control of escape behaviour. *Trends Cogn Sci*, 23(4):334-348

Evans DA, Stempel AV, Vale R, Ruehle S, Lefler Y, Branco T. (2018). A synaptic threshold mechanism for computing escape decisions. *Nature*, 558(7711):590-594

Feng J, Zhang C, Lischinsky JE, Jing M, Zhou J, Wang H, Zhang Y, Dong A, Wu Z, Wu H, Chen W, Zhang P, Zou J, Hires SA, Zhu JJ, Cui G, Lin D, Du J, Li Y. (2019). A genetically encoded fluorescent sensor for rapid and specific in vivo detection of norepinephrine. *Neuron*, 102(4):745-761.e8

Fernández-Pastor B, Ortega JE, Meana JJ. (2013). Involvement of serotonin 5-HT3 receptors in the modulation of noradrenergic transmission by serotonin reuptake inhibitors: a microdialysis study in rat brain. *Psychopharmacology (Berl)*, 229(2):331-44

Florin-Lechner SM, Druhan JP, Aston-Jones G, Valentino RJ. (1996). Enhanced norepinephrine release in prefrontal cortex with burst stimulation of the locus coeruleus. *Brain Res*, 742(1-2):89-97

Fratzl A, Koltchev AM, Vissers N, Tan YL, Marques-Smith A, Stempel AV, Branco T, Hofer SB. (2021). Flexible inhibitory control of visually evoked defensive behavior by the ventral lateral geniculate nucleus. *Neuron*,109(23):3810-3822

Ganella DE, Kim JH. (2014). Developmental rodent models of fear and anxiety: from neurobiology to pharmacology. *Br J Pharmacol*, 171(20):4556-74

Giustino TF, Maren S. (2018). Noradrenergic modulation of fear conditioning and extinction. *Front Behav Neurosci*, 12:43

Hu Y, Chen Z, Huang L, Xi Y, Li B, Wang H, Yan J, Lee TMC, Tao Q, So KF, Ren C. (2017). A translational study on looming-evoked defensive response and the underlying subcortical pathway in autism. *Sci Rep*, 7(1):14755

Huang L, Yuan T, Tan M, Xi Y, Hu Y, Tao Q, Zhao Z, Zheng J, Han Y, Xu F, Luo M, Sollars PJ, Pu M, Pickard GE, So KF, Ren C. (2017). A retinoraphe projection regulates serotonergic activity and looming-evoked defensive behaviour. *Nat Commun*, 8:14908

Ito R, Lee ACH. (2016). The role of the hippocampus in approach-avoidance conflict decision-making: Evidence from rodent and human studies. *Behav Brain Res*, 313:345-357

Kaehler ST, Singewald N, Philippu A. (1999). Dependence of serotonin release in the locus coeruleus on dorsal raphe neuronal activity. *Naunyn Schmiedebergs Arch Pharmacol,* 359(5):386-93

Kaye AP, Krystal JH. (2020). Predictive processing in mental illness: Hierarchical circuitry for perception and trauma. *Journal of Abnormal Psychology*, 129(6):629–632

Kim EJ, Kong MS, Park SG, Mizumori SJY, Cho J, Kim JJ. (2018). Dynamic coding of predatory information between the prelimbic cortex and lateral amygdala in foraging rats. *Sci Adv*, 4(4):eaar7328

Kirlic N, Young J, Aupperle RL. (2017). Animal to human translational paradigms relevant for approach avoidance conflict decision making. *Behav Res Ther*, 96:14-29

La-Vu M, Tobias BC, Schuette PJ, Adhikari A (2020). To approach or avoid: An introductory overview of the study of anxiety using rodent assays. *Frontiers in Behavioral Neuroscience*, 14, 145

Leger L, Descarries L. (1978). Serotonin nerve terminals in the locus coeruleus of adult rat: a radioautographic study. *Brain Res*, 145(1):1-13

Li L, Feng X, Zhou Z, Zhang H, Shi Q, Lei Z, Shen P, Yang Q, Zhao B, Chen S, Li L, Zhang Y, Wen P, Lu Z, Li X, Xu F, Wang L. (2018). Stress accelerates defensive responses to looming in mice and involves a locus coeruleus-superior colliculus projection. *Curr Biol*, 28(6):859-871

Li Y, Zhong W, Wang D, Feng Q, Liu Z, Zhou J, Jia C, Hu F, Zeng J, Guo Q, Fu L, Luo M. (2016). Serotonin neurons in the dorsal raphe nucleus encode reward signals. *Nat Commun*, 7:10503

Liu RJ, Aghajanian GK. (2008). Stress blunts serotonin- and hypocretin-evoked EPSCs in prefrontal cortex: role of corticosterone-mediated apical dendritic atrophy. *Proc Natl Acad Sci USA*, 105(1):359-64

Liu Z, Zhou J, Li Y, Hu F, Lu Y, Ma M, Feng Q, Zhang JE, Wang D, Zeng J, Bao J, Kim JY, Chen ZF, El Mestikawy S, Luo M. (2014). Dorsal raphe neurons signal reward through 5-HT and glutamate. *Neuron*, 81(6):1360-1374

Marcinkiewcz CA, Mazzone CM, D'Agostino G, Halladay LR, Hardaway JA, DiBerto JF, Navarro M, Burnham N, Cristiano C, Dorrier CE, Tipton GJ, Ramakrishnan C, Kozicz T, Deisseroth K, Thiele TE, McElligott ZA, Holmes A, Heisler LK, Kash TL. (2016). Serotonin engages an anxiety and fear-promoting circuit in the extended amygdala. *Nature*, 537(7618):97-101

Marzo A, Totah NK, Neves RM, Logothetis NK, Eschenko O. (2014). Unilateral electrical stimulation of rat locus coeruleus elicits bilateral response of norepinephrine neurons and sustained activation of medial prefrontal cortex. *J Neurophysiol*, 111(12):2570-88

Massé F, Hascoët M, Dailly E, Bourin M. (2006). Effect of noradrenergic system on the anxiolytic-like effect of DOI (5-HT2A/2C agonists) in the four-plate test. *Psychopharmacology (Berl)*, 183(4):471-81

Mathis A, Mamidanna P, Cury KM, Abe T, Murthy VN, Mathis MW, Bethge M. (2018). DeepLabCut: markerless pose estimation of user-defined body parts with deep learning. *Nat Neurosci*, 21(9):1281-1289

Miller SM, Marcotulli D, Shen A, Zweifel LS. (2019). Divergent medial amygdala projections regulate approach-avoidance conflict behavior. *Nat Neurosci*, 22(4):565-575

Nanez J. (1988). Perception of impending collision in 3-to 6-week-old human infants. *Infant Behavior and Development*, 11(4):447-463

Ortega JE, Mendiguren A, Pineda J, Meana JJ. (2012). Regulation of central noradrenergic activity by 5-HT(3) receptors located in the locus coeruleus of the rat. *Neuropharmacology*, 62(8):2472-9

Park YG, Sohn CH, Chen R, McCue M, Yun DH, Drummond GT, Ku T, Evans NB, Oak HC, Trieu W, Choi H, Jin X, Lilascharoen V, Wang J, Truttmann MC, Qi HW, Ploegh HL, Golub TR, Chen SC, Frosch MP, Kulik HJ, Lim BK, Chung K. (2018). Protection of tissue physicochemical properties using polyfunctional crosslinkers. *Nat Biotechnol*, 10.1038/nbt.4281

Pickel VM, Joh TH, Reis DJ. (1977). A serotonergic innervation of noradrenergic neurons in nucleus locus coeruleus: demonstration by immunocytochemical localization of the transmitter specific enzymes tyrosine and tryptophan hydroxylase. *Brain Res*, 131(2):197-214

Ranjbar-Slamloo Y, Fazlali Z. (2020). Dopamine and Noradrenaline in the Brain; Overlapping or Dissociate Functions? *Frontiers in Molecular Neuroscience*, 12:334

Ren C, Tao Q. (2020). Neural Circuits Underlying Innate Fear. *Adv Exp Med Biol*, 1284:1-7

Ren J, Friedmann D, Xiong J, Liu CD, Ferguson BR, Weerakkody T, DeLoach KE, Ran C, Pun A, Sun Y, Weissbourd B, Neve RL, Huguenard J, Horowitz MA, Luo L. (2018). Anatomically

Defined and Functionally Distinct Dorsal Raphe Serotonin Sub-systems. *Cell*, 175(2):472-487.e20

Ritter A, Habusha S, Edut S, Klavir O. (2022). Prefrontal Control of Innate Escape Behavior – A Neural Mechanism of Enhanced Posttraumatic Threat Detection. *BioRxiv*, 2022.12.21.521361

Salamone JD, Correa M, Yang JH, Rotolo R, Presby R. (2018). Dopamine, effort-based choice, and behavioral economics: Basic and translational research. *Frontiers in Behavioral Neuroscience*,12:25

Salamone JD, Correa M. (2012) The mysterious motivational functions of mesolimbic dopamine. *Neuron*, 76(3):470-85

Salay LD, Ishiko N, Huberman AD. (2018). A midline thalamic circuit determines reactions to visual threat. *Nature*, 557(7704):183-189

Schiff W, Caviness JA, Gibson JJ. (1962). Persistent fear responses in rhesus monkeys to the optical stimulus of "looming". *Science*, 136(3520):982-3

Schultz W, Dickinson A. (2000). Neuronal coding of prediction errors. *Annu Rev Neurosci*, 23:473-500

Schultz W. (2010). Dopamine signals for reward value and risk: basic and recent data. *Behav Brain Funct*, 6:24

Schultz W. (2016). Dopamine reward prediction error coding. *Dialogues Clin Neurosci*, 18(1):23-32

Sciolino NR, Hsiang M, Mazzone CM, Wilson LR, Plummer NW, Amin J, Smith KG, McGee CA, Fry SA, Yang CX, Powell JM, Bruchas MR, Kravitz AV, Cushman JD, Krashes MJ, Cui G, Jensen P. (2022). Natural locus coeruleus dynamics during feeding. *Sci Adv*, 8(33):eabn9134

Shang C, Chen Z, Liu A, Li Y, Zhang J, Qu B, Yan F, Zhang Y, Liu W, Liu Z, Guo X, Li D, Wang Y, Cao P. (2018). Divergent midbrain circuits orchestrate escape and freezing responses to looming stimuli in mice. *Nat Commun*, 9(1):1232

Shang C, Liu Z, Chen Z, Shi Y, Wang Q, Liu S, Li D, Cao P. (2015). A parvalbumin-positive excitatory visual pathway to trigger fear responses in mice. *Science*, 348(6242):1472-7

Silva BA, Gross CT, Gräff J. (2016). The neural circuits of innate fear: detection, integration, action, and memorization. *Learn Mem*, 23(10):544-55

Su Z, Cohen J. (2022). Two types of locus coeruleus norepinephrine neurons drive reinforcement learning. *BioRxiv*, 2022.12.08.519670

Sun F, Zeng J, Jing M, Zhou J, Feng J, Owen SF, Luo Y, Li F, Wang H, Yamaguchi T, Yong Z, Gao Y, Peng W, Wang L, Zhang S, Du J, Lin D, Xu M, Kreitzer AC, Cui G, Li Y. (2018). A genetically encoded fluorescent sensor enables rapid and specific detection of dopamine in flies, fish, and mice. *Cell*, 174(2):481-496.e19

Sun F, Zhou J, Dai B, Qian T, Zeng J, Li X, Zhuo Y, Zhang Y, Wang Y, Qian C, Tan K, Feng J, Dong H, Lin D, Cui G, Li Y. (2020). Next-generation GRAB sensors for monitoring dopaminergic activity in vivo. *Nat Methods*, 17(11):1156-1166

Szabo ST, Blier P. (2001). Serotonin (1A) receptor ligands act on norepinephrine neuron firing through excitatory amino acid and GABA(A) receptors: a microiontophoretic study in the rat locus coeruleus. *Synapse*, 42(4):203-12

Ungless MA. (2004). Dopamine: the salient issue. *Trends Neurosci*, 27(12):702-6

van der Weel FR, van der Meer AL. (2009). Seeing it coming: infants' brain responses to looming danger. *Naturwissenschaften*, 96(12):1385-91

Vander Weele CM, Siciliano CA, Matthews GA, Namburi P, Izadmehr EM, Espinel IC, Nieh EH, Schut EHS, Padilla-Coreano N, Burgos-Robles A, Chang CJ, Kimchi EY, Beyeler A, Wichmann R, Wildes CP, Tye KM. (2018). Dopamine enhances signal-to-noise ratio in cortical-brainstem encoding of aversive stimuli. *Nature*, 563(7731):397-401

Varazzani C, San-Galli A, Gilardeau S, Bouret S. (2015). Noradrenaline and dopamine neurons in the reward/effort trade-off: a direct electrophysiological comparison in behaving monkeys. *J Neurosci*, 35(20):7866-77

Ventura R, Latagliata EC, Morrone C, La Mela I, Puglisi-Allegra S. (2008). Prefrontal norepinephrine determines attribution of "high" motivational salience. *PLoS One*, 3(8):e3044

Wan J, Peng W, Li X, Qian T, Song K, Zeng J, Deng F, Hao S, Feng J, Zhang P, Zhang Y, Zou J, Pan S, Shin M, Venton BJ, Zhu JJ, Jing M, Xu M, Li Y. (2021). A genetically encoded sensor for measuring serotonin dynamics. *Nat Neurosci*, 24(5):746-752

Wei P, Liu N, Zhang Z, Liu X, Tang Y, He X, Wu B, Zhou Z, Liu Y, Li J, Zhang Y, Zhou X, Xu L, Chen L, Bi G, Hu X, Xu F, Wang L. (2015). Processing of visually evoked innate fear by a non-canonical thalamic pathway. *Nat Commun*, 6:6756

Yilmaz M, Meister M. (2013). Rapid innate defensive responses of mice to looming visual stimuli. *Curr Biol*, 23(20):2011-5

Yu AJ, Dayan P. (2005). Uncertainty, neuromodulation, and attention. *Neuron*, 46(4):681-92

Zald DH, Treadway MT. (2017). Reward processing, neuroeconomics, and psychopathology. *Annu Rev Clin Psychol*, 13:471-495

Zambetti PR, Schuessler BP, Kim JJ. (2019). Sex Differences in Foraging Rats to Naturalistic Aerial Predator Stimuli. *iScience*, 16:442-452

Zambetti PR, Schuessler BP, Lecamp BE, Shin A, Kim EJ, Kim JJ. (2022). Ecological analysis of Pavlovian fear conditioning in rats. *Commun Biol*, 5(1):830

Zhao X, Liu M, Cang J. (2014). Visual cortex modulates the magnitude but not the selectivity of looming-evoked responses in the superior colliculus of awake mice. *Neuron*, 84(1):202-213

Zhou Z, Liu X, Chen S, Zhang Z, Liu Y, Montardy Q, Tang Y, Wei P, Liu N, Li L, Song R, Lai J, He X, Chen C, Bi G, Feng G, Xu F, Wang L. (2019). A VTA GABAergic neural circuit mediates visually evoked innate defensive responses. *Neuron*, 103(3):473-488

Zhu Y, Dewell RB, Wang H, Gabbiani F. (2018). Pre-synaptic muscarinic excitation enhances the discrimination of looming stimuli in a collision-detection neuron. *Cell Rep*, 23(8):2365-2378

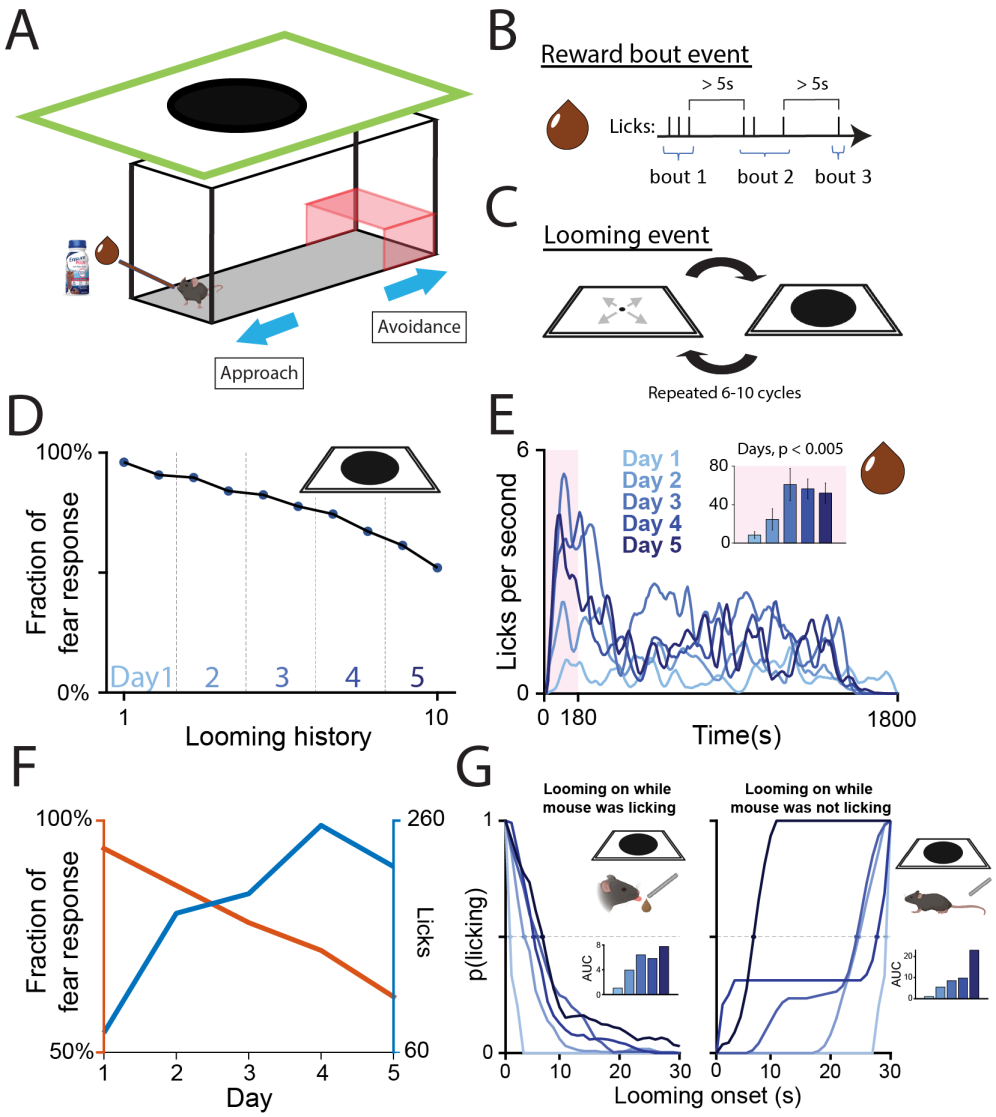

Figure 1. A naturalistic motivational conflict task which assesses reward foraging and innate fear responses. **A**: Diagram of the approach/avoidance conflict task setting. Each mouse is allowed to freely lick for reward (Ensure), but with unexpected looming stimuli present from above. **B**: Event of a reward bout, which is defined as a train of continuous licks within 5 seconds from last lick. **C**: Event of the Looming stimulus, which is displayed as a quick expanding black disk mimicking an approaching aerial predator. **D**: Percentage of fear responses induced by looming stimuli across five daily days (n = 25). **E**: Lick distribution (in Hz) across 5 daily sessions. Inset figure indicates a one-way ANOVA analysis with the average licks (±S.E.M.) within the first 180 seconds (pink background) each day. **F**: Adaptive behavior indicated by a multiple scale of fear response and number of licks. **G**: Event of looming stimulus was presented while the mouse was licking (left) versus not licking (right panel). Inset figures represent the area under the curve (AUC) each day.

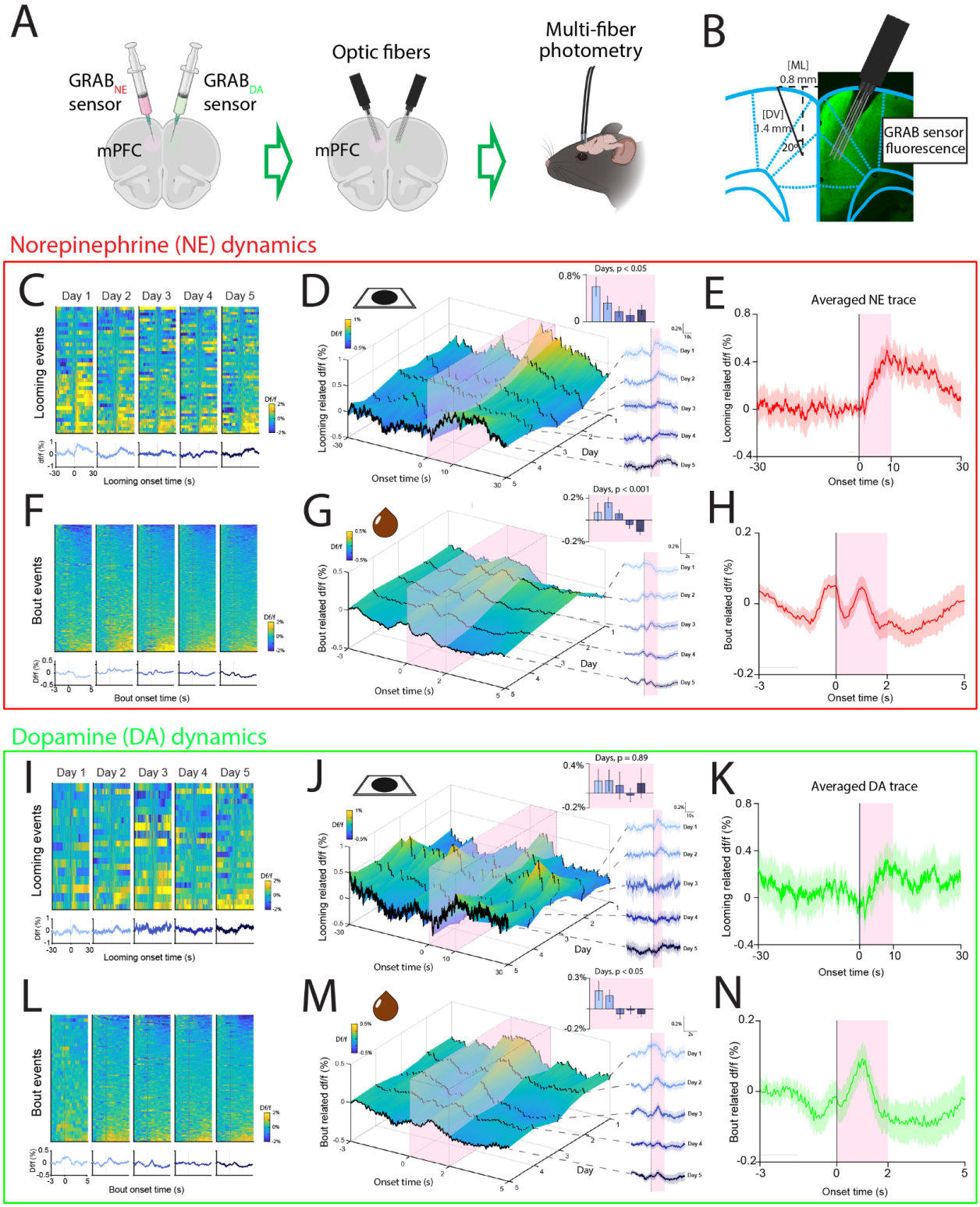
A
GRAB NE sensor
GRAB DA sensor
mPFC
Optic fibers
mPFC
Multi-fiber photometry
B
[ML]
0.8 mm
[DV]
1.4 mm
20°
GRAB sensor fluorescence
Norepinephrine (NE) dynamics
C
Day 1
Day 2
Day 3
Day 4
Day 5
Looming events
Looming onset time (s)
D
Days, p < 0.05
Looming related df/f (%)
Onset time (s)
Day
E
Averaged NE trace
Looming related df/f (%)
Onset time (s)
F
Bout events
Bout onset time (s)
G
Days, p < 0.001
Bout related df/f (%)
Onset time (s)
Day
H
Bout related df/f (%)
Onset time (s)
Dopamine (DA) dynamics
I
Day 1
Day 2
Day 3
Day 4
Day 5
Looming events
Looming onset time (s)
J
Days, p = 0.89
Looming related df/f (%)
Onset time (s)
Day
K
Averaged DA trace
Looming related df/f (%)
Onset time (s)
L
Bout events
Bout onset time (s)
M
Days, p < 0.05
Bout related df/f (%)
Onset time (s)
Day
N
Bout related df/f (%)
Onset time (s)

Figure 2. Multi-fiber photometry with GRAB sensors for measuring *in vivo* event-dependent neuromodulators dynamics. **A**: Diagram of bilateral GRAB sensor injections and optic fiber implements targeted mouse mPFC. **B**: Example histology photo of GRAB sensor expression and fiber track with a 20° angle. **C-H**: Event-related norepinephrine (NE) dynamics to looming stimuli and reward bouts. **C**: Heatmaps (top) of looming-induced individual NE traces 30 seconds before and after event onset (t = 0) and average (bottom) across days. **D**: Three-dimension representation of day-by-day looming-related NE dynamic change across each daily session (right). Shaded area indicates the 95% of confidence intervals. Inset figure indicates a one-way ANOVA analysis of mean NE activity (±S.E.M.) within the 0 to 10s window (pink background). **E**: Averaged NE trace of all looming events. **F**: Heatmaps of reward-bout-induced individual NE traces (top) and average (bottom) across days. **G**: Three-dimension representation of bout-related averaged NE dynamic across each daily session (right). Inset figure indicates a one-way ANOVA analysis of mean NE activity within the 0 to 2s window. **H**: Averaged NE trace of all bout events. **I-N**: Event-related dopamine (DA) dynamics to looming stimuli and reward bouts.

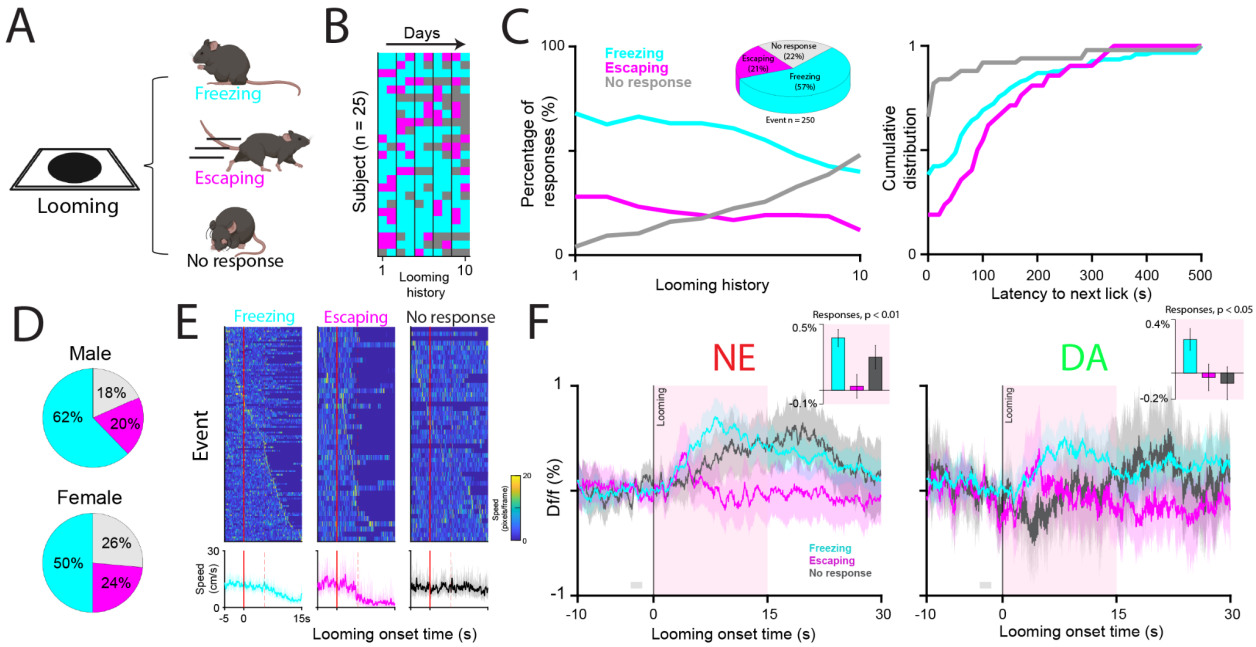

Figure 3. Dissociative neuromodulatory dynamics between looming-induced freezing and escaping behavior. **A**: Diagram of looming-induced responses, including freezing, escaping, and no response. **B**: Heatmap representation of individual mouse (n = 25) response across looming stimuli. **C**: (Left) Percentage of freezing, escaping, and no response over 10 looming stimuli. Piechart represents the overall ratio of behavioral responses. (Right) Cumulative distribution of latency to next lick after freezing, escaping, and no response behavioral subtypes. **D**: Percentage of looming-induced behavior responses between male (n = 15) and female (n = 10) mice. **E**: Heatmaps of looming-induced freezing (left), escaping (middle), and no response (right) on speed changes in a -5 to 15s window from looming onset (red line). (Bottom) Averaged speed (±95% confidence interval) from each day. **F**: Norepinephrine (left) and dopamine (right) dynamic changes associated with looming-induced responses. Shaded area indicates the 95% of confidence intervals. Inset figure represents a one-way ANOVA analysis of averaged df/f (±S.E.M.) within the 0 to 15s window (pink background).

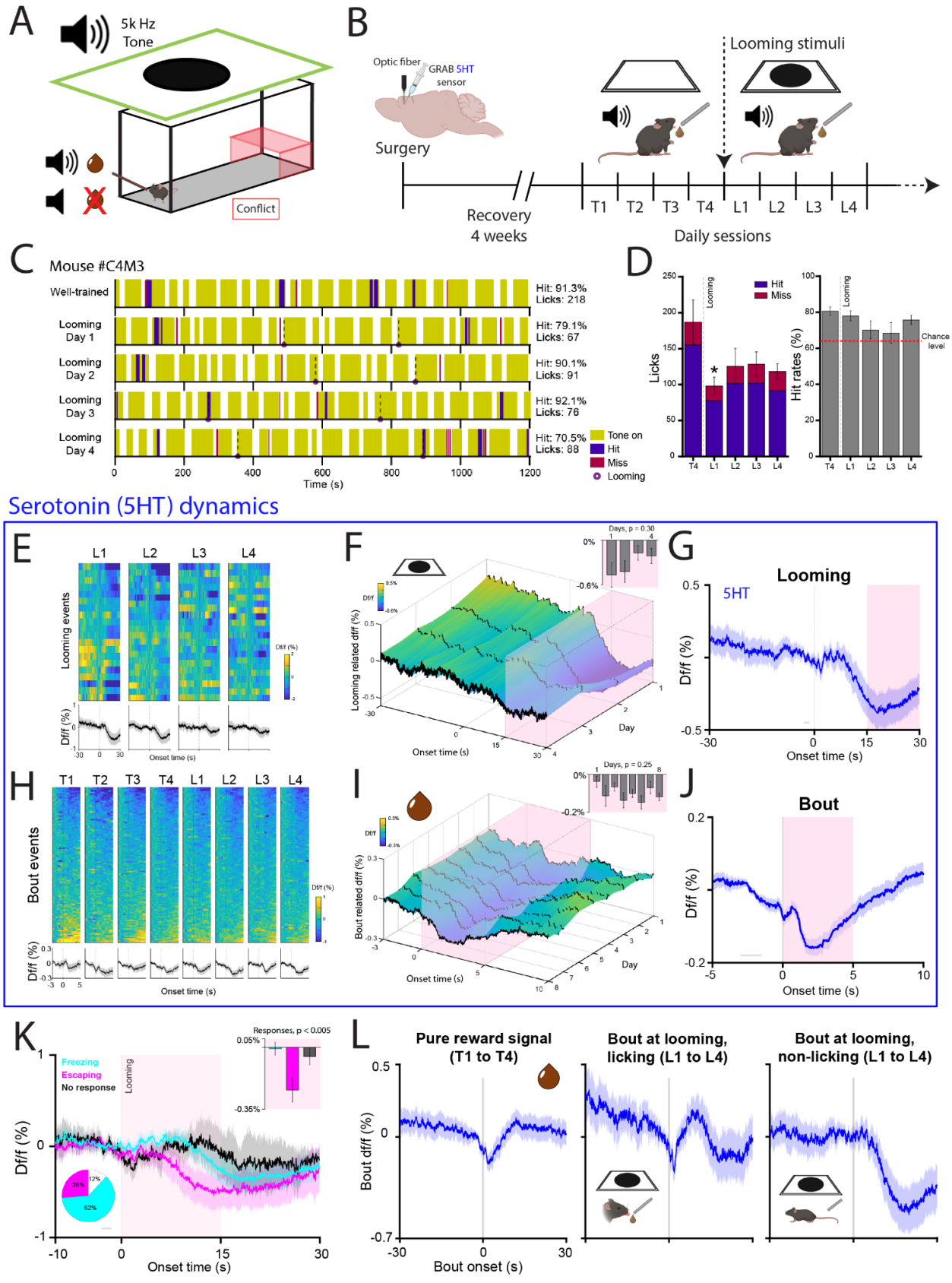
A
5k Hz
Tone
Conflict
B
Optic fiber
GRAB 5HT
sensor
Surgery
Looming stimuli
Recovery
4 weeks
T1 T2 T3 T4 L1 L2 L3 L4
Daily sessions
C
Mouse #C4M3
Well-trained
Hit: 91.3%
Licks: 218
Looming Day 1
Hit: 79.1%
Licks: 67
Looming Day 2
Hit: 90.1%
Licks: 91
Looming Day 3
Hit: 92.1%
Licks: 76
Looming Day 4
Hit: 70.5%
Licks: 88
Tone on
Hit
Miss
Looming
Time (s)
D
Licks
Hit
Miss
Looming
Hit rates (%)
Chance level
Serotonin (5HT) dynamics
E
L1 L2 L3 L4
Looming events
Df/f (%)
Onset time (s)
F
Looming related df/f (%)
Onset time (s)
Day
Days, p = 0.30
G
Looming
5HT
Df/f (%)
Onset time (s)
H
T1 T2 T3 T4 L1 L2 L3 L4
Bout events
Df/f (%)
Onset time (s)
I
Bout related df/f (%)
Onset time (s)
Day
Days, p = 0.25
J
Bout
Df/f (%)
Onset time (s)
K
Freezing
Escaping
No response
Looming
Responses, p < 0.005
Df/f (%)
Onset time (s)
L
Pure reward signal
(T1 to T4)
Bout at looming,
licking (L1 to L4)
Bout at looming,
non-licking (L1 to L4)
Bout df/f (%)
Bout onset (s)

Figure 4. Serotonin (5HT) dynamics in a tone version of conflict task. **A**: Diagram of a tone component added in the approach/avoidance conflict task. Tone-on indicates reward availability and potential looming stimuli. **B**: Experimental schema of the task. After surgery and recovery, the behavioral task is divided into 4 training (T1 to T4) and 4 looming days (L1 to L4). Looming stimuli are introduced only on L1 to L4. **C**: Example responses of a mouse performing the task in well-trained (T4) and looming days (L1 to L4). Licks during tone-on are recorded as 'hits', otherwise 'misses' during tone-off period. **D**: Average licks (left) and hit rates (right) on T1 and L1 to L4. *: $p < 0.05$ planned comparisons to T4. **E-J**: Event-related serotonin (5HT) dynamics to looming stimuli and reward bouts. **E**: Heatmaps (top) of looming-induced individual 5HT traces 30 seconds before and after event onset (t = 0) and average (bottom) across 4 looming days. Shaded area indicates the 95% of confidence intervals. **F**: Three-dimension representation of looming-related 5HT dynamics over days. Inset figure indicates a one-way ANOVA analysis of mean 5HT activity (±S.E.M.) within the 15 to 30s window (pink background). **G**: Averaged 5HT trace of all looming events. **H**: Heatmaps of reward-bout-induced individual 5HT traces (top) and average (bottom) across days. **I**: Three-dimension representation of bout-related averaged NE dynamic across each daily session. Inset figure indicates a one-way ANOVA analysis of mean 5HT activity within the 0 to 5s window. **J**: Averaged 5HT trace of all bout events. **K**: 5HT dynamics associated with looming-induced freezing, escaping, and no response. Inset figure represents a one-way ANOVA analysis of averaged df/f (±S.E.M.) within the 0 to 15s window (pink background). **L**: Averaged 5HT traces (±95% confidence interval) of pure reward signal (T1 to T4, left). 5HT activity to bout events between mouse keep licking when looming was on (middle) and mouse quit licking (right).

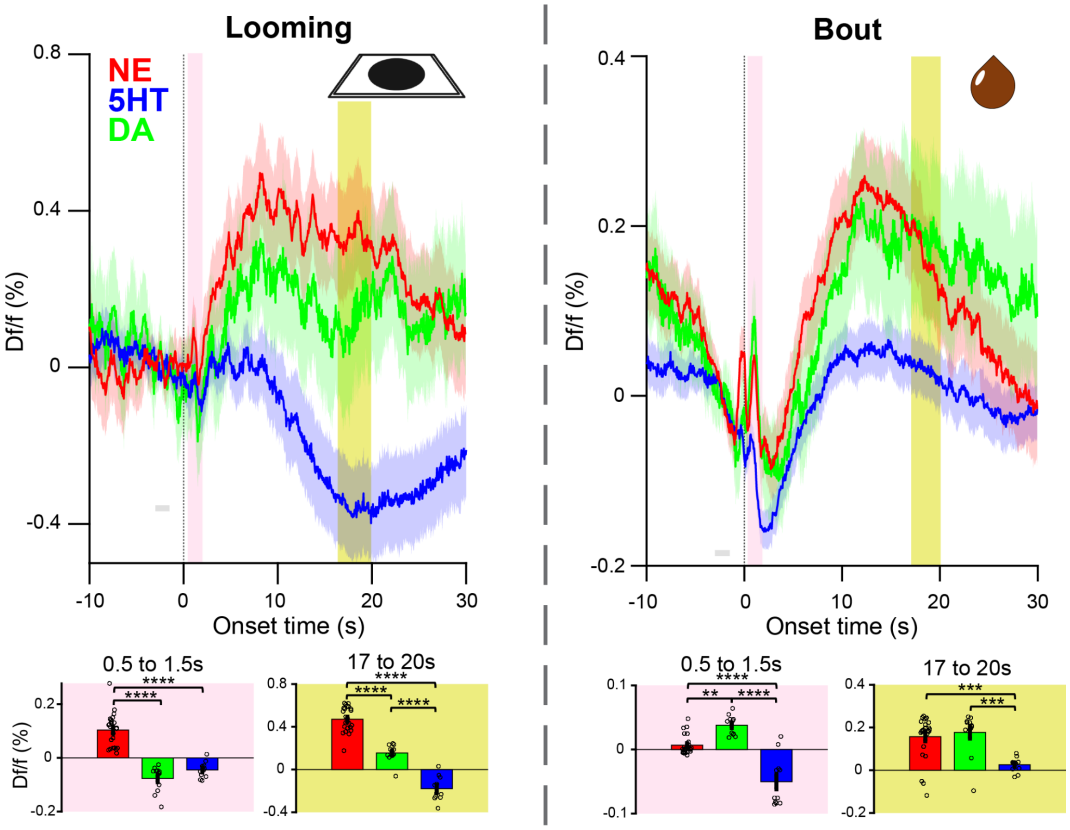

Figure 5. NE, DA, and 5HT showed dissociative dynamics toward negative (i.e. looming threat) and positive (reward bout) valences. Looming-related (left) and bout-related (right) traces across all daily sessions. (Bottom) One-way ANOVA analyses of averaged activities (±S.E.M.) from 0.5 to 1.5s (pink) and 17 to 20s (mustard yellow) windows. **: $p < 0.01$; ***: $p < 0.001$; ****: $p < 0.0001$, multiple comparisons with adjusted alpha value.

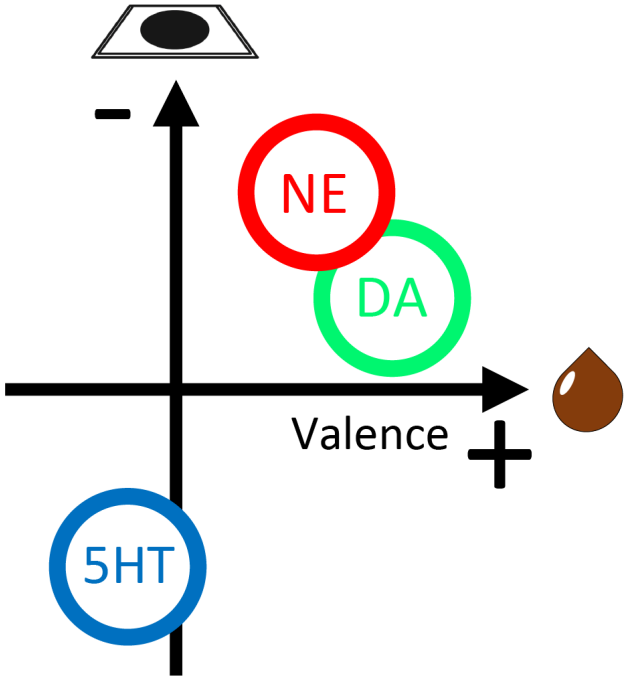

Figure 6. Schema of the roles of NE, DA, and 5HT in negative and positive valences. NE plays a more prominent role in representing threat (negative valence) and DA encodes reward (positive valence). In contrast, 5HT shows decreased activity to both valences.

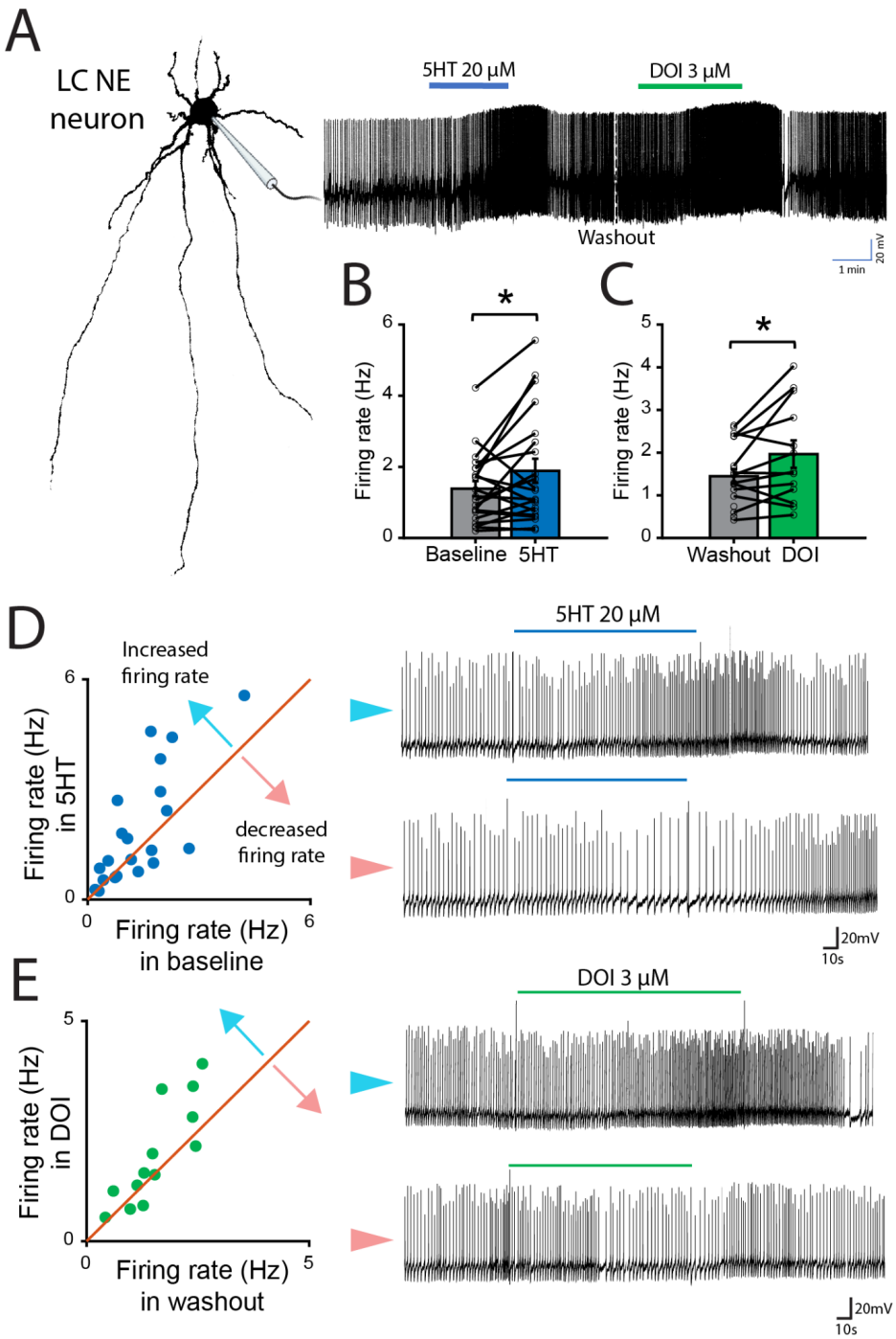

Figure 7. *Ex vivo* slice recording of locus coeruleus (LC) NE neurons with 5HT-related treatments. **A**: Diagram of patch clamp recording of an example LC NE cell body and its spontaneous activity. **B**: Spontaneous spikes of LC NE neurons after 5HT (20 μM), and **C**: a $5HT_{2A/2C}$ agonist DOI (3 μM) treatment. *: $p < 0.05$, paired t-test. **D:** Sub-population of LC NE neurons showed heterogeneous firing rate to 5HT (left). Example cells showing increased (top) and decreased (bottom) firing rate. **E:** Heterogeneous firing rate of LC NE neurons to DOI.

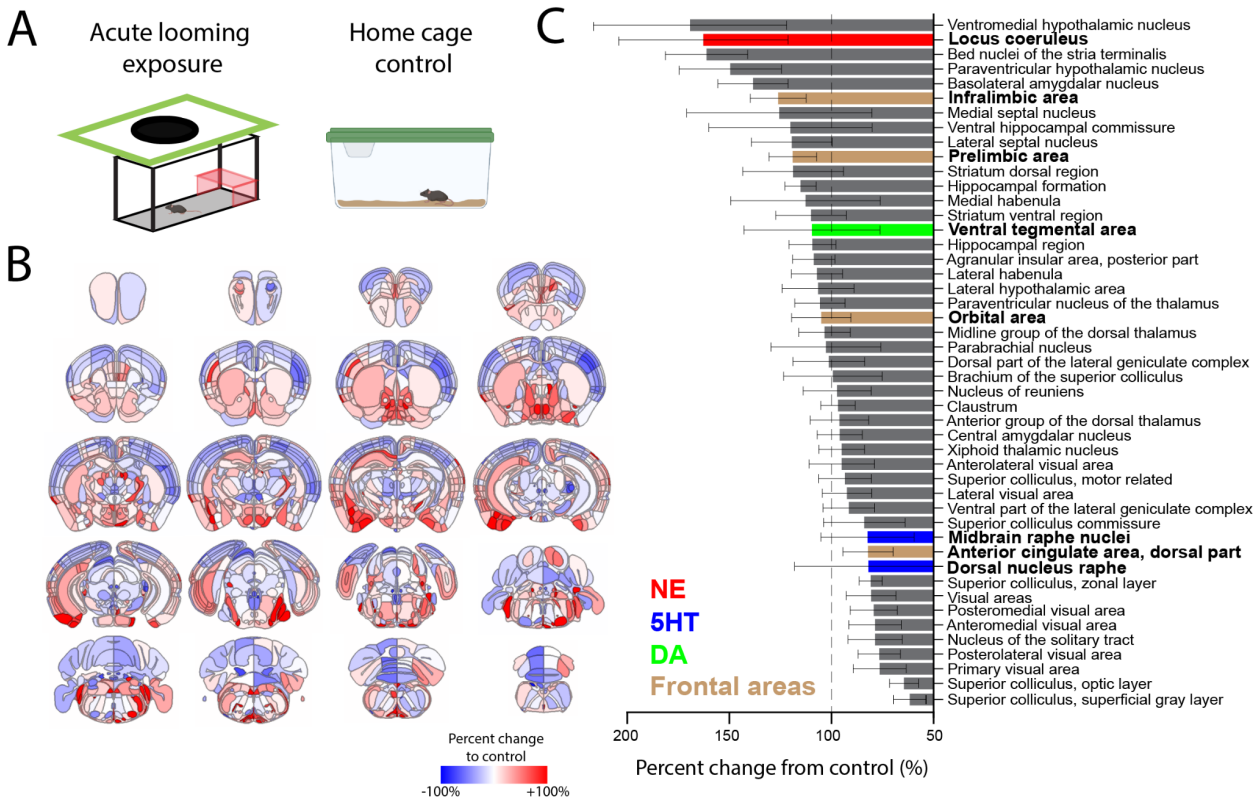

Figure S1. Whole-brain cFos mapping. **A**: Samples were collected from mice that experienced looming stimuli (left, n = 6), and baselined with a home cage control group (right, n = 6). **B**: averaged cFos expression in example coronal slices is shown in percent change of density from control (±S.E.M.). **C**: A list of regions of interest relating to looming stimulus.

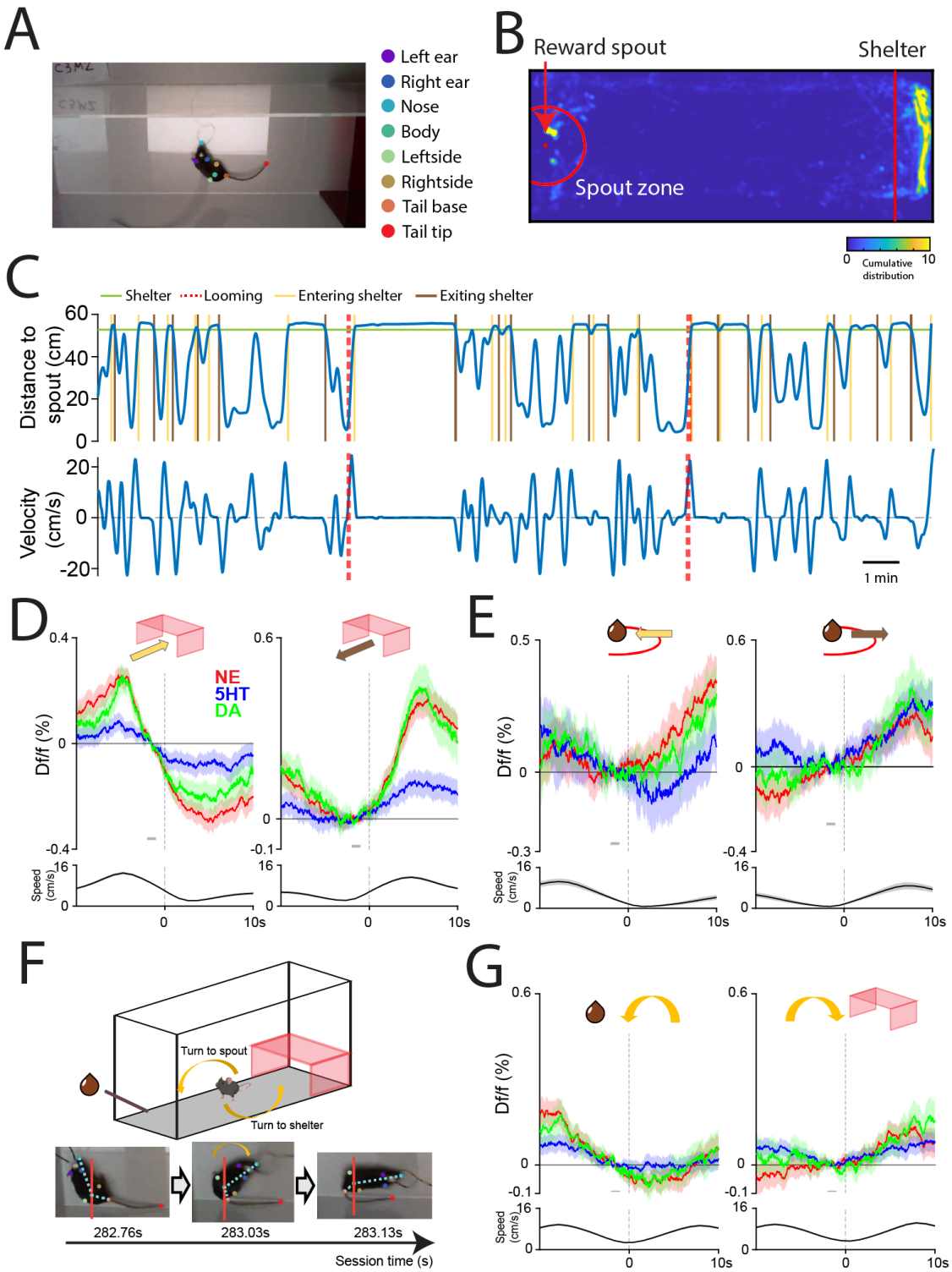

Figure S2. Behavioral events tracking by using a supervised deep learning model (Deeplabcut). **A**: An example frame of a mouse performing the task with labeled body parts. **B**: Heatmap of mouse position in cumulative distribution. The red dot represents the reward spout location, and the red circle represents the spout zone, which is defined as a radius of 10% of box length. And

the red line represents the entering edge of the shelter. **C**: Example trace of a mouse traveling in the box in a daily session. Mouse position is shown by distance to spout (top) and running velocity (bottom). **D**: Neuromodulator activity at events of entering (left) and exiting (right) the shelter. Bottom panels represent the running speed. Shaded area indicates the 95% of confidence intervals. **E**: Neuromodulator activity at events of entering (left) and exiting (right) spout zone. **F**: A diagram illustrates turning to spout versus turning to shelter. (Bottom) Example frames of a mouse making a turn. **G**: Neuromodulator activity at events of turn to spout (left) and turn to shelter (right) spout zone.

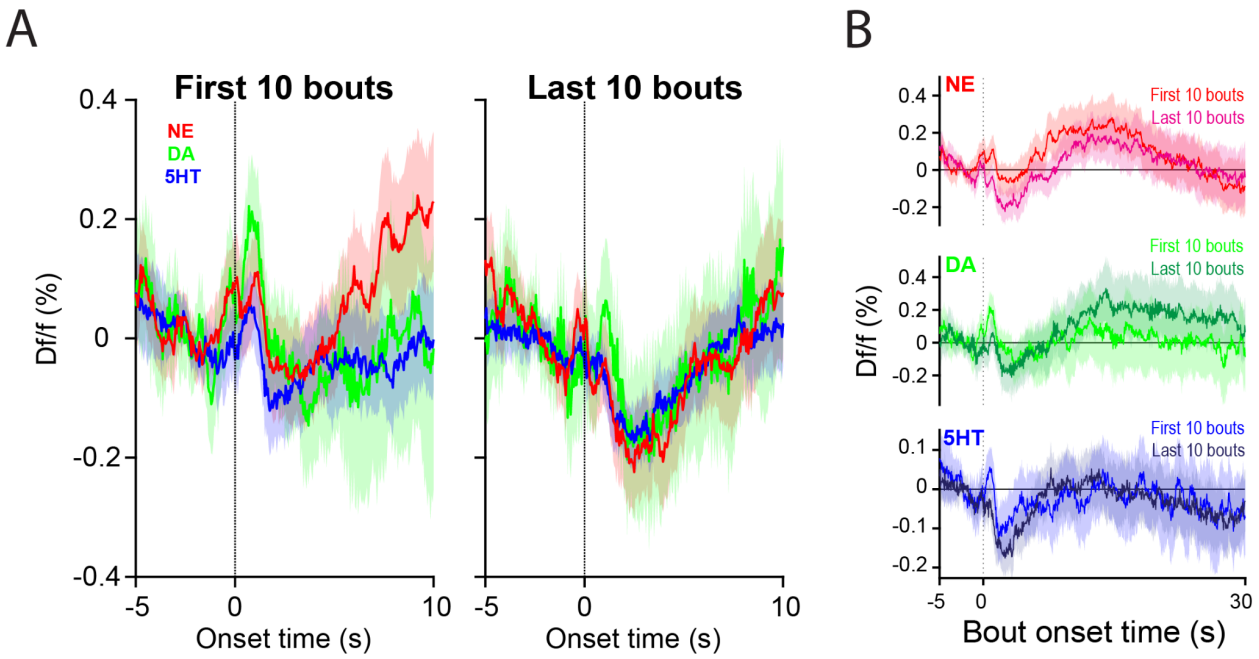

Figure S3. Neuromodulator activities respond to different bout states. **A**: Averaged NE, DA, and 5HT associated with the first 10 (left) and the last 10 bout (right). **B**: Visualization of the first versus last 10 bouts in NE (top), DA (middle), and 5HT (bottom) dynamics. Shaded area indicates the 95% of confidence intervals.

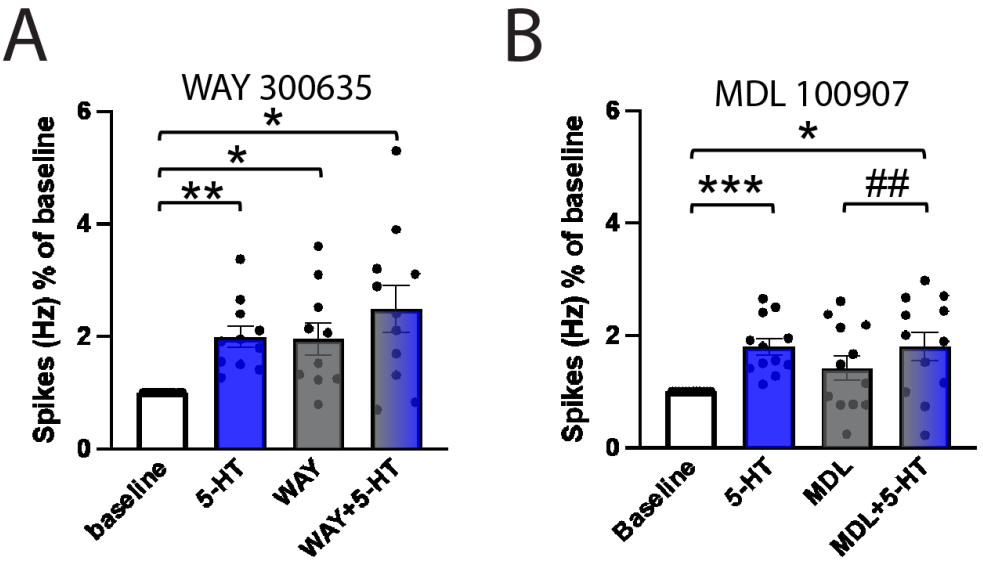

Figure S4. Effects of 5HT-related bath applications on LC NE neuron activity *ex vivo*. **A**: Effects of WAY300635, a $5HT_{1A}$ antagonist, on LC NE neurons spikes. **B**: Effects of MDL100907, a $5HT_{2A}$ antagonist, on LC NE neurons spikes. *: $p < 0.05$; **: $p < 0.01$; ***: $p < 0.005$, chi-square test. ##: $p < 0.01$, paired t-test.